

1 **Muted orbital-scale Monsoon Variability over the Korean**
2 **Peninsula**

3 Nitesh Sinha^{1,2}, Axel Timmermann^{1,2}, Sun-Seon Lee^{1,2}, Kyoung-Nam Jo³, Jasper A. Wassenburg^{1,2}, Daniel
4 M. Cleary^{1,2}, Kyung-Sook Yun^{1,2}

5

6 ¹Center for Climate Physics, Institute for Basic Science, Busan, Republic of Korea

7 ²Pusan National University, Busan, Republic of Korea

8 ³Kangwon National University, Chuncheon, Gangwon-do, Republic of Korea

9

10 Correspondence to: nitesh@pusan.ac.kr

11

12

13

14

15

16

17

18

19

20 **This file includes:**

21

22 Figures S1 to S15

23 Section S1-S2

24 Table S1

25 Table S2

26 SI References

27

28 **Section S1: Tagging Experiment**

29

30 The water tagging experiment has been conducted with the iCESM and we used the following source
 31 regions (Figure S7):

32

33 **Land Tagging:**

34

35 **SAS** - South Asia, **CAS** - Central Asia, **TAS** - Tropical Asia, **EAS** - East Asia, **NAS** - North Asia,
 36 **AFR** – Africa, **EUR** – Europe, **LND** – All land.

37

38

39 **Ocean Tagging:**

40

41 **NNP** - northern North Pacific, **SNP** - subtropical North Pacific, **EEP** - east equatorial Pacific, **WEP** -
 42 west equatorial Pacific, **SSP** - subtropical South Pacific, **EQI** - equatorial Indian, **SSI** - subtropical
 43 South Indian.

44

45 P is the total precipitation at the target location (KP) with contributions P_i from all the tagged source
 46 regions.

47

48

49

$$P = \sum_{i=1}^n P_i$$

50

51

52 $\delta^{18}O_p$ at a particular grid cell is the sum of precipitation- $\delta^{18}O_i$ originating from all tagged
 53 source regions (i), weighted by their precipitation contribution:

54

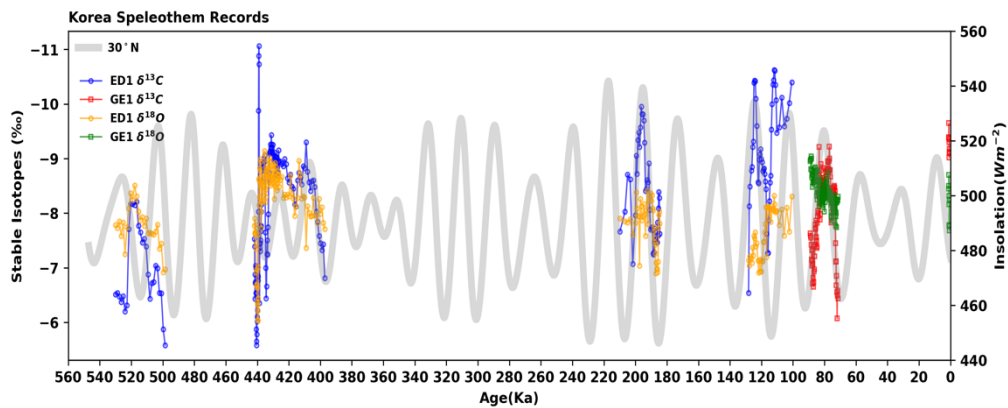
55

$$\delta^{18}O_p = \sum_{i=1}^n \delta^{18}O_i \frac{P_i}{P}$$

56

57

58



59

60

61 **Fig. S1.** Speleothem ($\delta^{13}C$ and $\delta^{18}O$) records from Eden Cave (ED1) and Gwaneum Cave (GE1) in South Korea.
 62 Refer to Jo et al. (Jo et al., 2011, 2014) for further details.

63

64

65

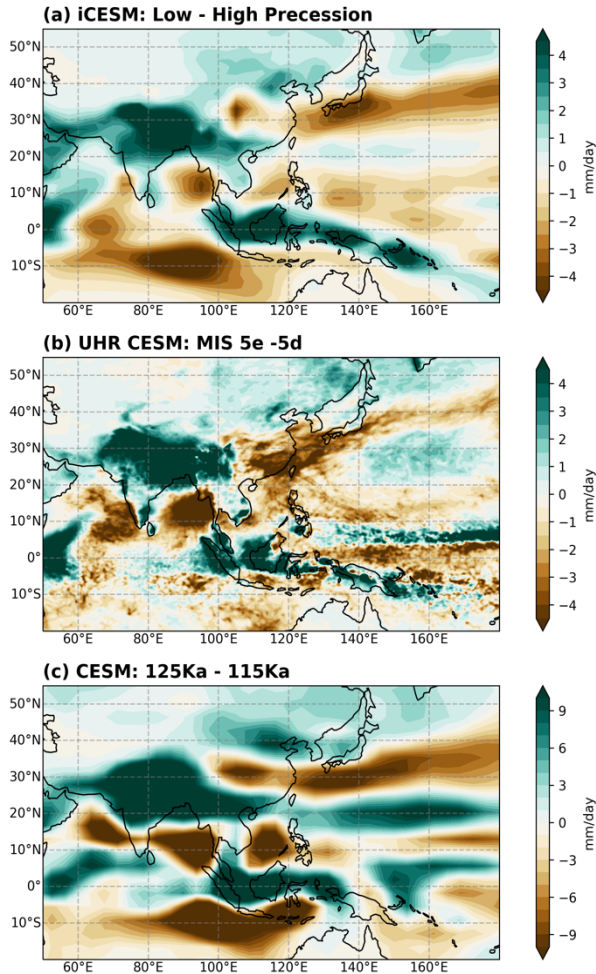


Fig. S2. Summer mean precipitation differences for (a) Low – High precession from iCESM simulation ($\sim 2^\circ$ horizontal resolution), (b) MIS5e – MIS5d from ultra-high-resolution (UHR) CESM simulations ($\sim 0.25^\circ$ horizontal resolution), and (c) time slices for 125 ka – 115 ka from 3Ma transient simulation. ($\sim 3.75^\circ$ horizontal resolution),

66
67
68
69

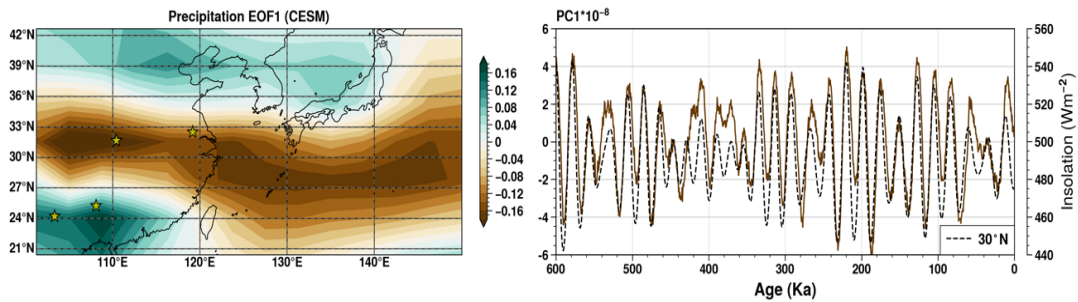


Fig. S3. First empirical orthogonal function (EOF1) for annual mean precipitation (shaded, left panel) and corresponding principal component (PC1) (brown curve, right panel) for Eastern Asia using 3Ma transient simulation. The EOF analysis is based on the last 600 kyr of the simulation. Major studied caves in China are marked by a yellow star symbol (left panel), refer to Figure 1. The black dashed curve represents summer insolation at 30°N (right panel).

70
71
72
73
74

75 Section S2

76

77 Beck's(Beck et al., 2018) ^{10}Be reconstruction corresponds well to simulated regional rainfall
 78 over the Loess area if we shift the ^{10}Be record by ~ 6 ka (Fig. S4c). The shifted ^{10}Be shows a
 79 higher correlation ($R^2 = 0.30$) with the simulated rainfall than the reported $R^2 = 0.16$ with the
 80 Sanbao $\delta^{18}\text{O}_{\text{sp}}$ record. The ^{10}Be record (6 ka shifted) also matches quite well with Cryptomeria
 81 pollen records from Japan(Hayashi et al., 2021; Igarashi and Oba, 2006) (Figure 3c). Now, we
 82 understand that the precipitation and $\delta^{18}\text{O}_p$ spatial patterns as a grand dipole response to orbital
 83 forcing(Wen et al., 2024). The age shift may be justified as ^{10}Be age determination uses one of
 84 the assumptions that the Chinese speleothem- $\delta^{18}\text{O}$ record was controlled by regional EASM
 85 rainfall intensity. Moreover, our model simulations also do not support the EASM precipitation
 86 and $\delta^{18}\text{O}_p$ uniform temporal or spatial relationship throughout the region on orbital timescales,
 87 such as Chinese speleothem- $\delta^{18}\text{O}$ does not correspond well with simulated China rainfall but
 88 with India rainfall (Fig. S4a and S4b).

89

90

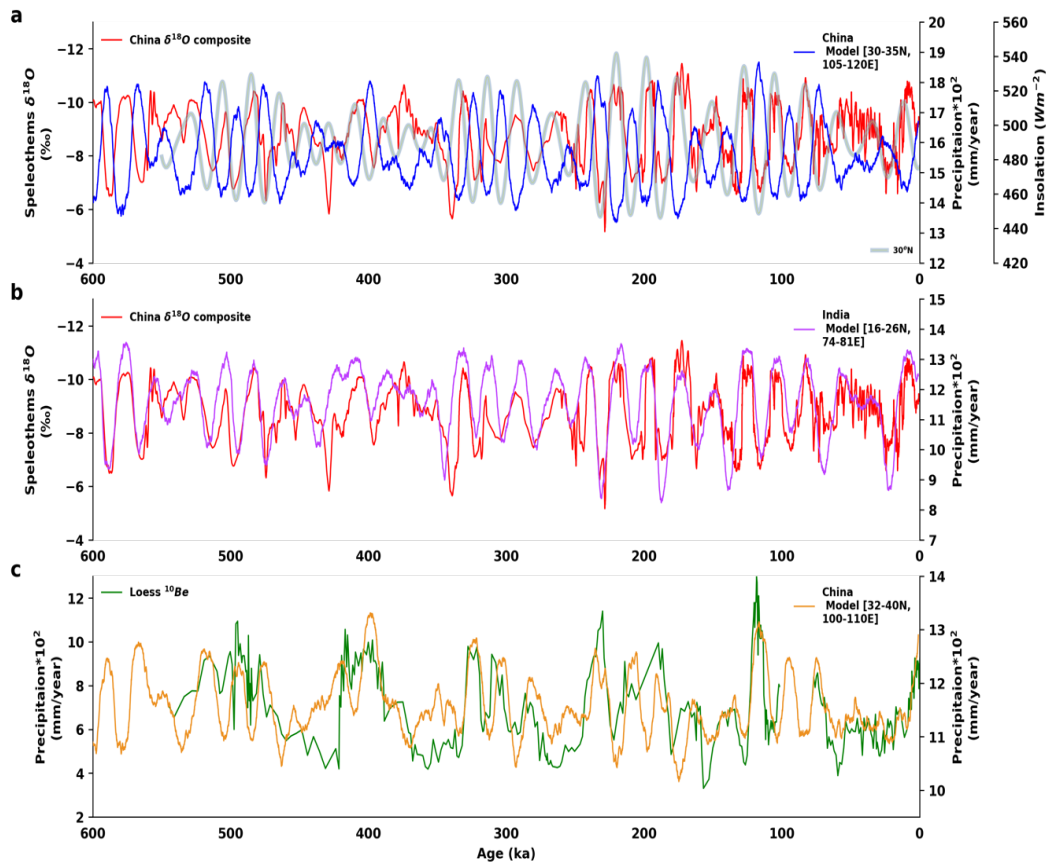


Fig. S4. Comparison of simulated precipitation change by 3 Ma transient simulation (only the last 600 kyr are shown here) and proxies from (a) Eastern Asia and China speleothem- $\delta^{18}\text{O}$ composite record, (b) India and China speleothem- $\delta^{18}\text{O}$ composite record, and (c) China and Loess ^{10}Be record. Summer insolation at 30°N is shown in panel (a).

91

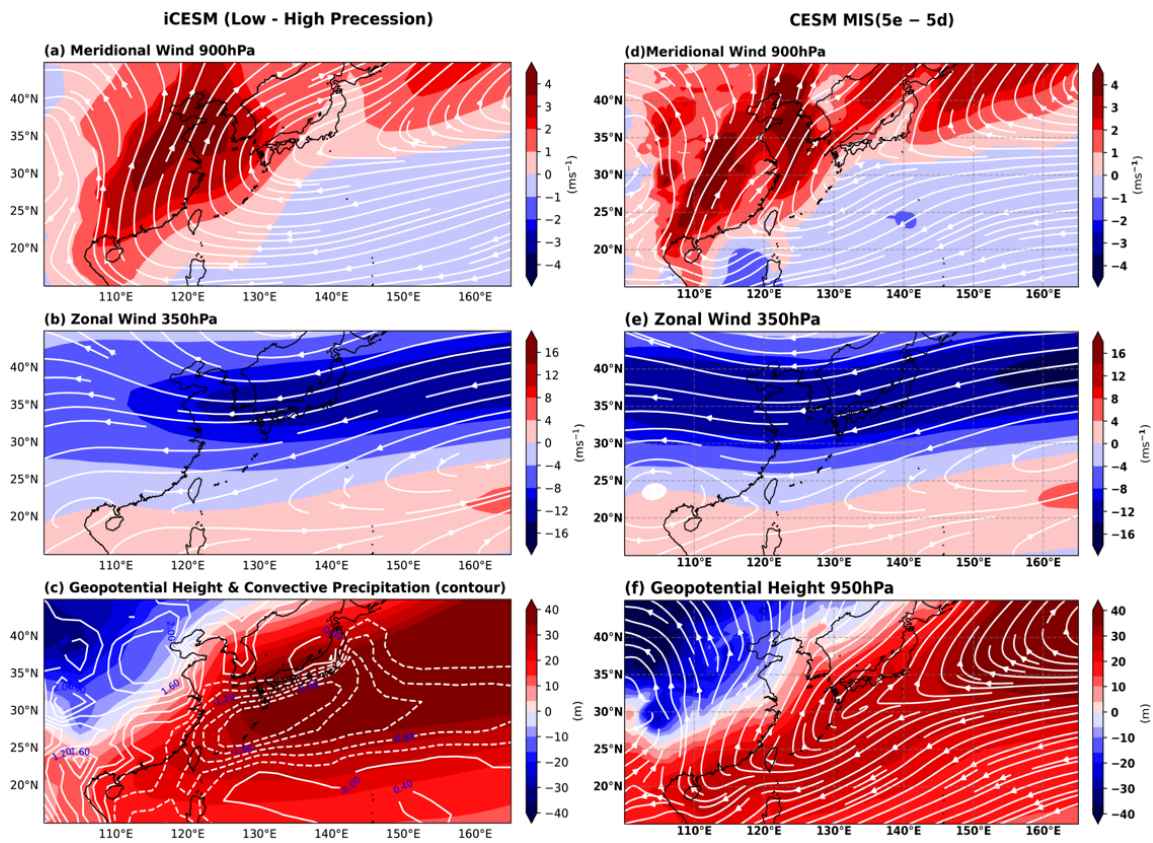
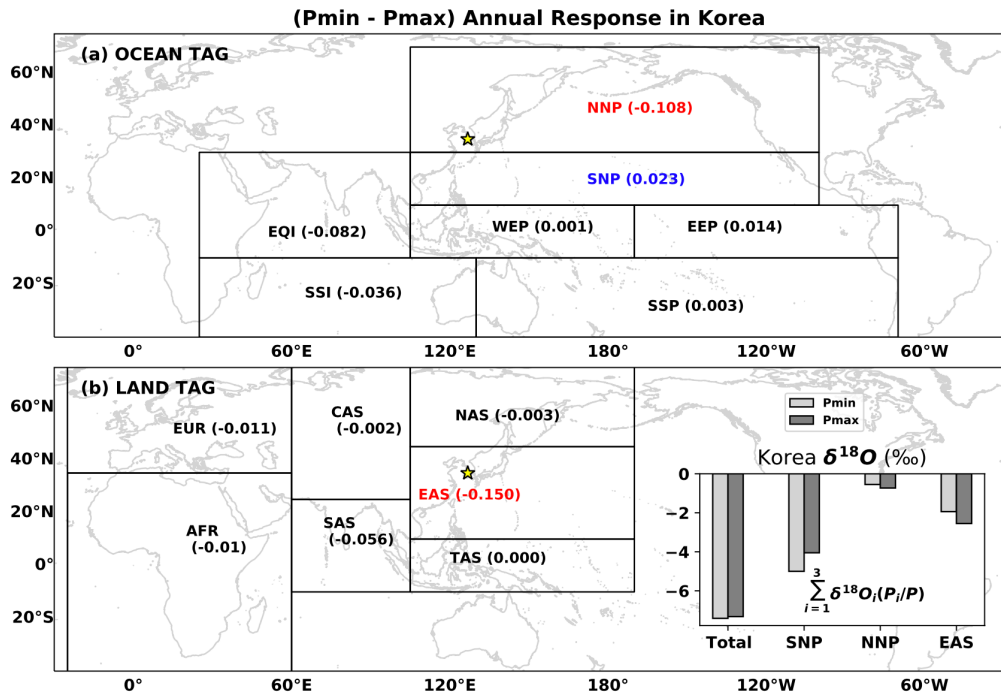
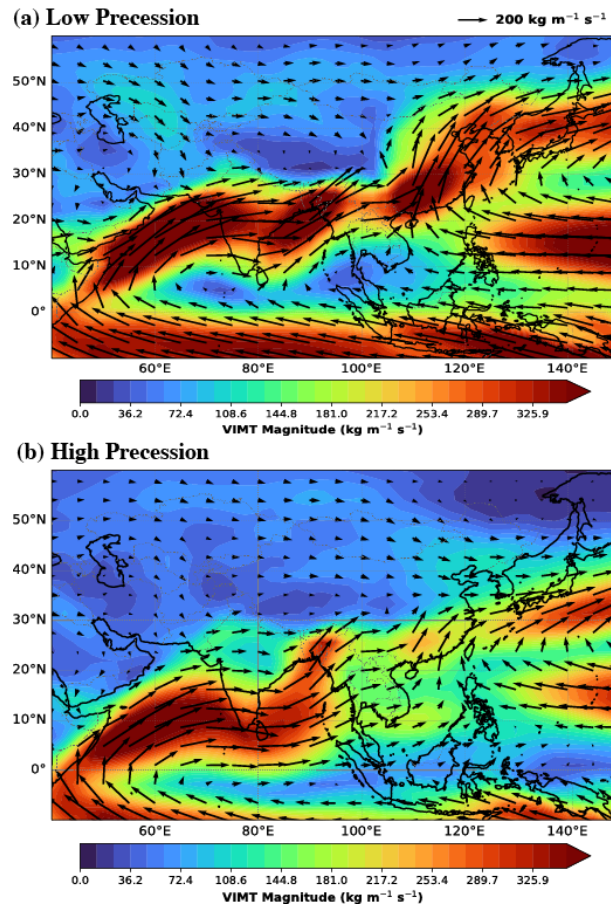


Fig. S5. Differences between P_{min} and P_{max} in iCESM-130ka (left panels) and between hiresCESM-5d and hiresCESM-5e (right panels). (a)(d) Meridional wind at 900 hPa (shading) and streamlines. (b)(e) Zonal wind at 350 hPa (shading) and streamlines. (c) Geopotential height 950 hPa (shading) and convective precipitation (contour). (f) Geopotential height 950 hPa (shading) and streamlines.



94
95
96
97
98
99
100
101

Figure S6: Differences in annual precipitation (mm/day) on the Korean Peninsula between P_{min} and P_{max} from various moisture sources over (a) ocean and (b) land. Color text is a major contributor to the Korean Peninsula (blue positive and red negative for $P_{min} - P_{max}$). Inset plot (lower right): the summer precipitation $\delta^{18}O$ in Korea from major and near-source contributors from Land (EAS) and the Ocean (SNP, NNP). “Total” represents the precipitation- $\delta^{18}O$ combination from all tag regions in Korea. Korea is marked by a yellow star.



103
 104
 105
 106
 107
 108

Fig. S7. Vertically integrated moisture transport (VIMT) during boreal summer (JJA) under low precession (a) and high precession (b) conditions. VIMT magnitude ($\text{kg m}^{-1} \text{s}^{-1}$) showing the spatial distribution and intensity of moisture transport across Asia. Black arrows indicate VIMT vector direction and relative magnitude (reference vector: $200 \text{ kg m}^{-1} \text{s}^{-1}$).

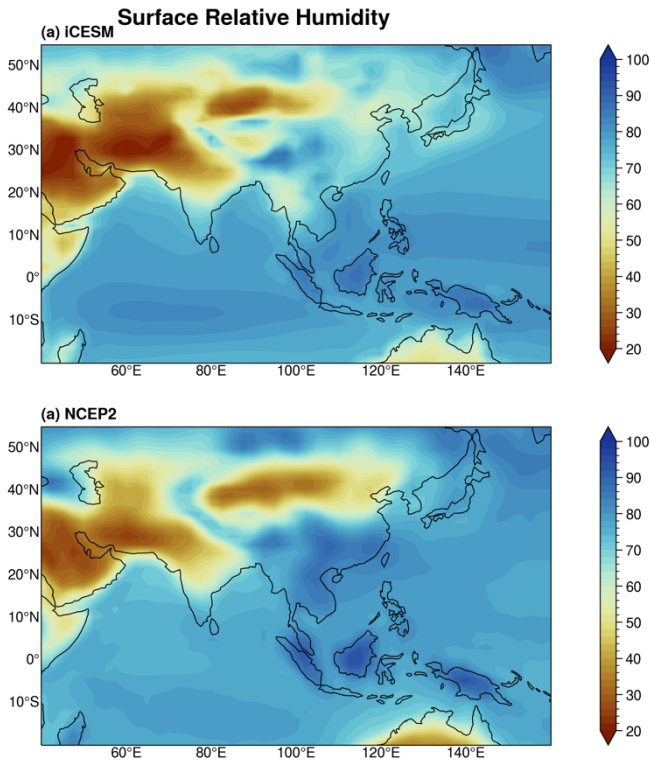


Fig. S8. (a) Relative humidity simulated in iCESM for present day conditions in comparison to (b) NCEP2 reanalysis data for the last 40 years (accessed through APDRC OPeNDAP Server (<http://apdrc.soest.hawaii.edu/index.php>)). Model captures the spatial pattern reasonably well, except lower humidity over the southeast Asian region.

109
110
111
112

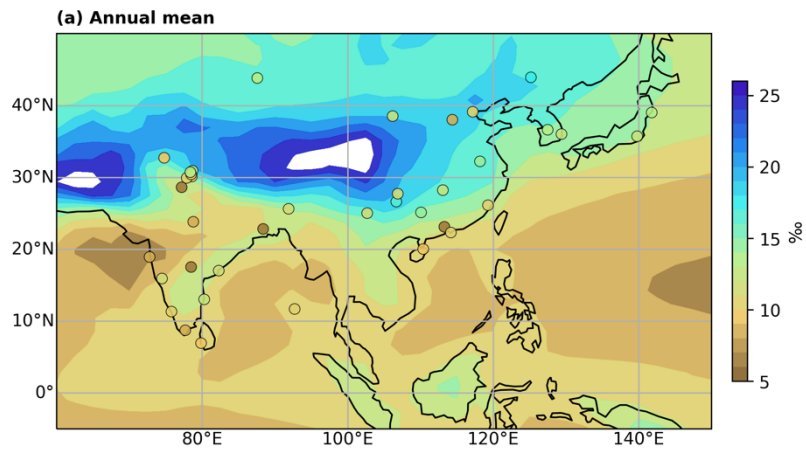


Fig. S9. Present day iCESM simulated (shaded) d-excess and GNIP sites (circle) annual mean d-excess comparison.

113

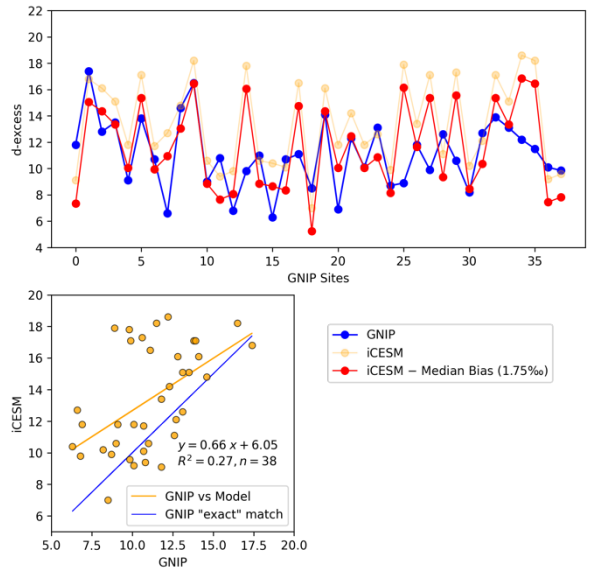


Fig. S10. Upper panel shows the series of d -excess values for 38 Asian sites, GNP (blue), iCESM (orange), and iCESM Median bias adjusted (red). Lower left panel shows the correlation between simulated and GNP mean annual d -excess values for Asian sites. Note: All Asian GNP sites are considered here, a screening has been applied, such as only the sites which have at least 2 years of data.

114
115
116

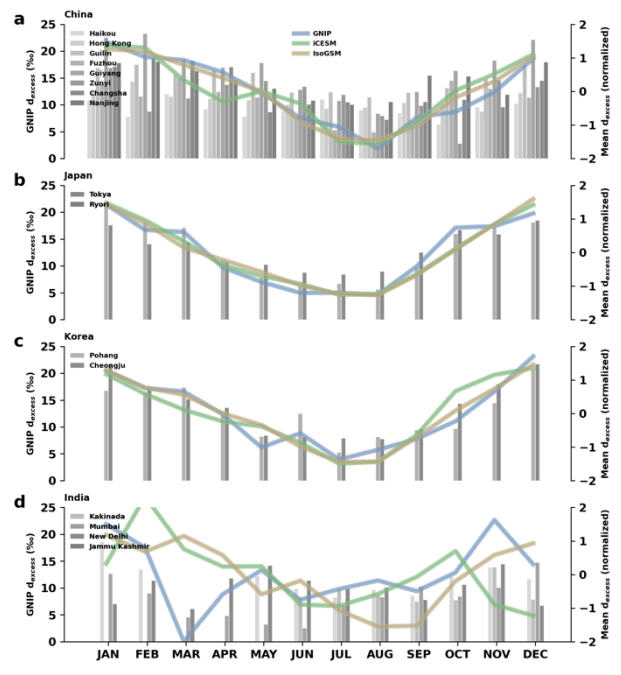
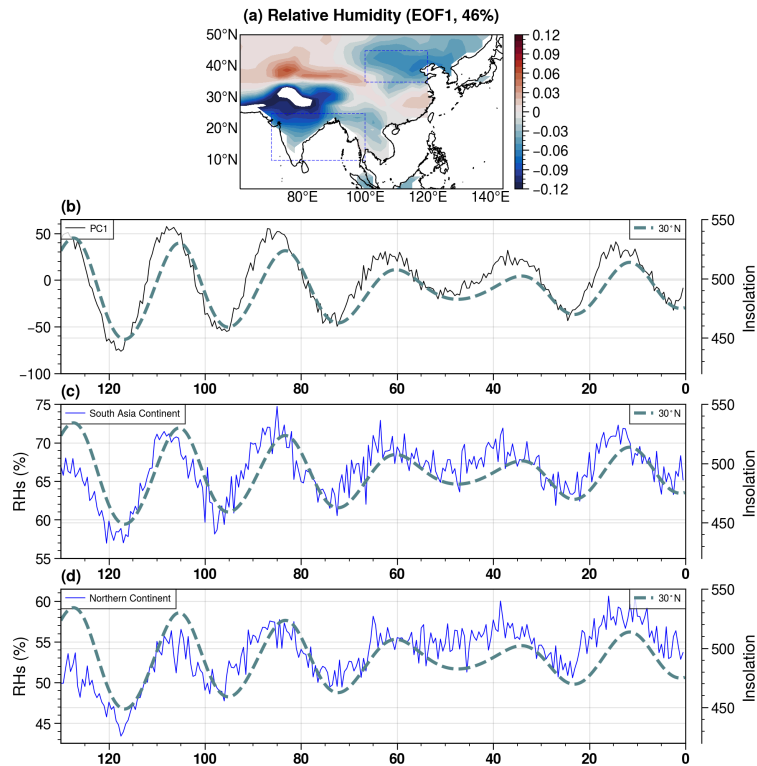


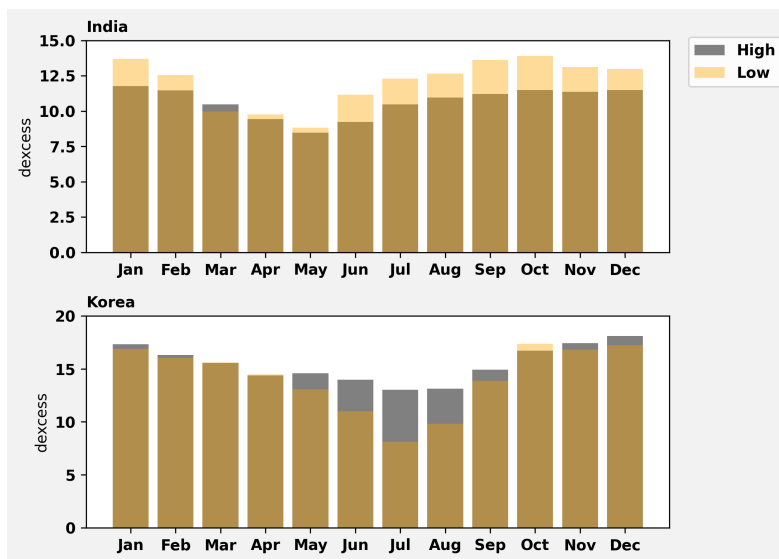
Fig. S11. A comparison between the monthly climatology of d -excess from GNP (light blue), iCESM simulation (light green), and IsoGSM2 (light brown) for some of the sites from China, Japan, Korea, and India. Gray bars show mean monthly d -excess for individual GNP sites, gray shading represents site latitude from low to high (lighter to darker).

117
118
119
120
121
122



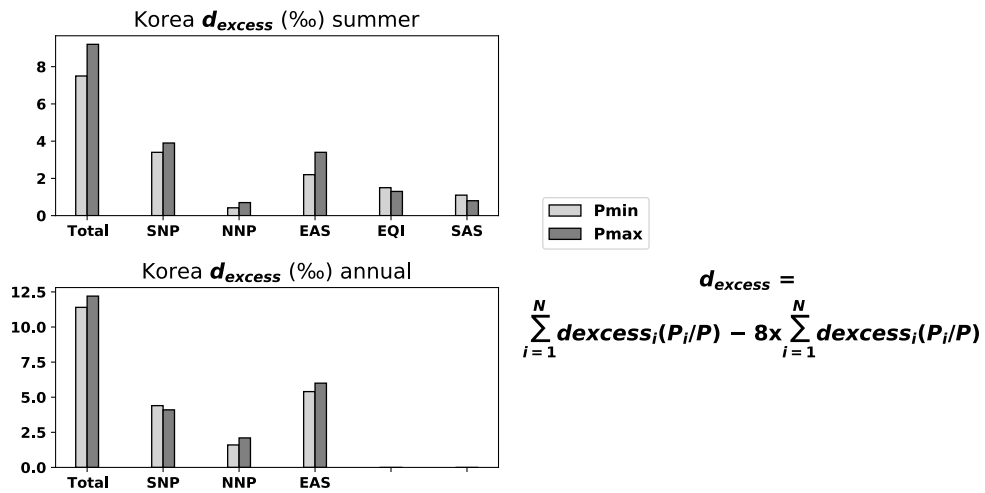
123
124
125
126
127
128
129
130
131
132
133
134
135

Fig. S12. First empirical orthogonal function (EOF1(a)) and corresponding principal component (PC1, b) for the summer mean surface relative humidity for the 130 ka transient simulation on iCESM1.2. Temporal evolution of surface relative humidity over continental regions (c, d). The selected boxes are shown on the spatial map (a). The dashed curve represents summer insolation at 30°N. It is worth mentioning here that the EAS region in the tagging experiments covers the Chinese continent up to 45°N and 100°E.



136
137
138
139
140

Fig. S13. *d*-excess monthly climatology for low precession (Low) and high precession (High) over the Indian and the Korean regions.



142
143
144
145
146
147
148

Figure S14: The summer and annual precipitation d -excess in Korea from major and near-source contributors from land and ocean. “Total” represents the d -excess from all tag regions to Korea.

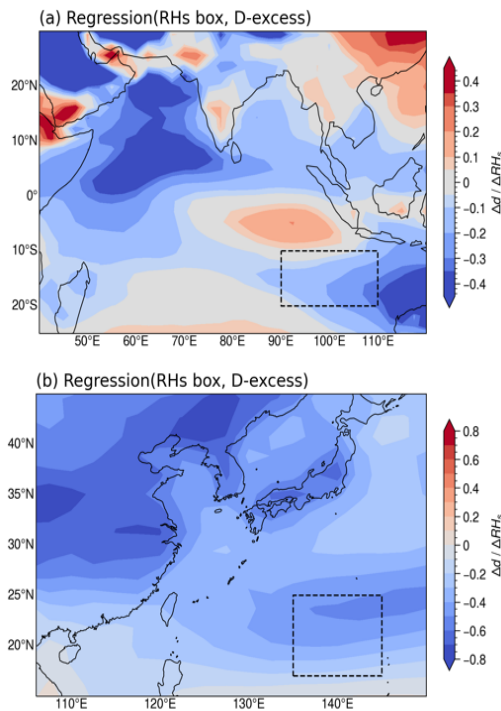
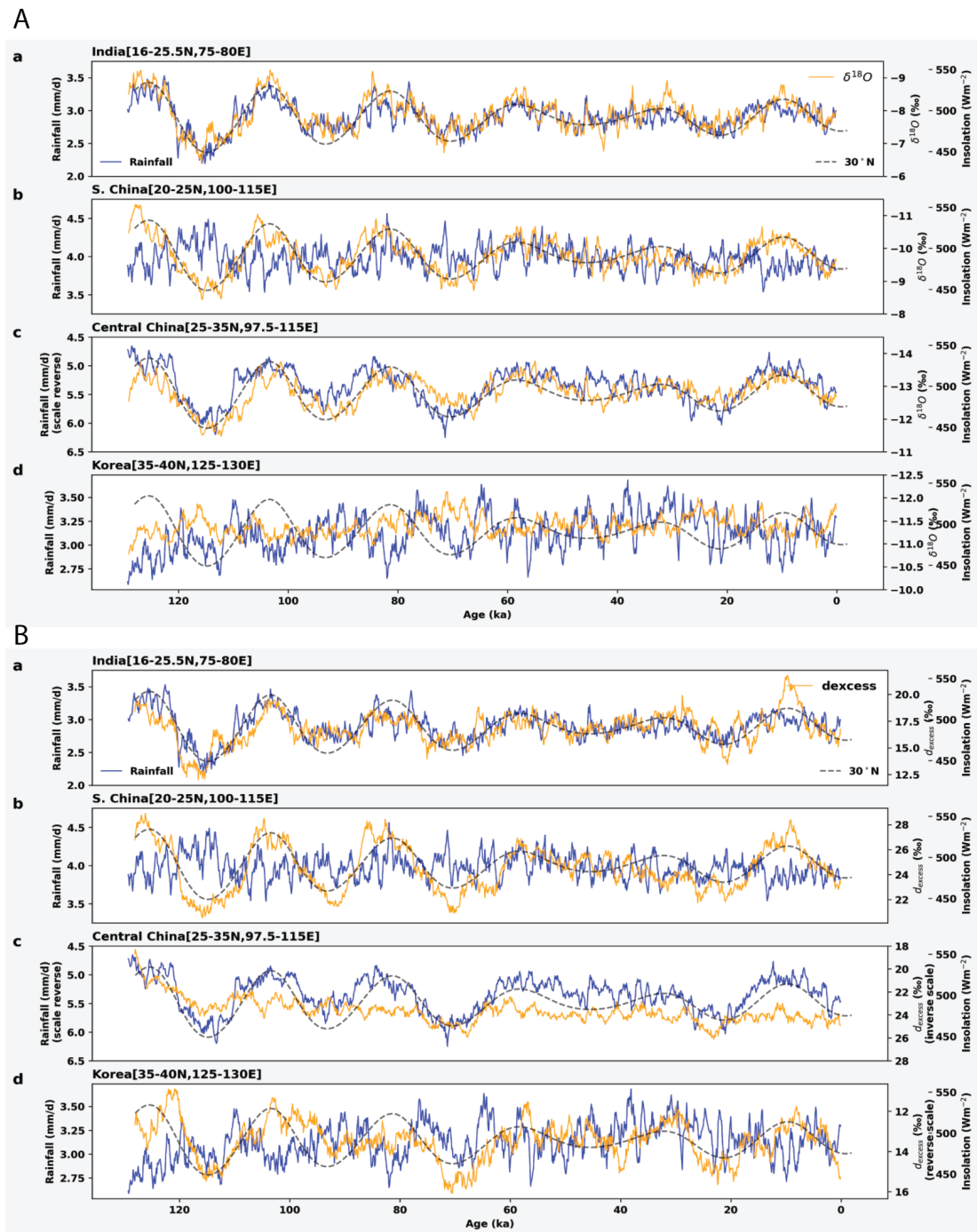


Fig. S15. (a) Southern Indian Ocean (10-20°S; 90-110°E) and (b) Northwest Pacific Ocean (15-25°N; 135-145°E) surface relative (Rel.) humidity (RHs) regressed over the spatial d -excess(d) values for 130 ka transient simulation. The shading shows slope; $\Delta d / \Delta RH_s$.



151
152
153
154
155
156
157

Fig. S16. Simulated annual mean variations in precipitation (blue curves) for (a) India, (b) South (S.) China, (c) central China, and (d) Korea in the last 130ka from an orbitally forced transient simulation conducted with *iCESM1.2*. Orange curves in panel A (B) show precipitation- $\delta^{18}\text{O}$ (*d*-excess). Dashed black curves represent insolation (30°N) insolation changes.

158
159

Table S1: Details on the speleothem stable isotopes records and other proxies used in this study.

Speleothem-$\delta^{18}\text{O}$ records			
	~ Ages (ka)	Location ($^{\circ}\text{N}/^{\circ}\text{E}$)	Reference
<i>Korea</i>			
1. Eden cave (ED1)	100 – 128, 184 – 209, 397 – 442, 498 – 530	37.10/128.50	(Jo et al., 2011, 2014)
2. Gwaneum cave (GE1)	0.70 – 1.18, 71 – 89	37.32/129.03	
<i>China</i>			
1. Composite	0 – 640	several	(Cheng et al., 2016)
Other proxy records			
	~ Ages (ka)	Location ($^{\circ}\text{N}/^{\circ}\text{E}$)	Reference
1. Loess ^{10}Be	0 – 84 and 107 – 550	34.43/107.12	(Beck et al., 2018)
2. U1427 pollen	0.65 – 551	35.96/134.43	(Hayashi et al., 2021)
3. Lake Biwa	1.8 – 134.3 and 0 - 430	~35/~136	(Hayashi et al., 2017; Tarasov et al., 2011)
Atmospheric CO_2			
1. EPICA Dome CO_2	0-800	-75.1/158.72	(Lüthi et al., n.d.)

160

161
162
163

Table S2: Tagging results. Blank spaces indicate tag regions not used in the total calculation (column "Total"), as they have no contribution to the anomalous $\delta^{18}O_p$ (Pmin- Pmax).

(a) d18O																	
Annual	SNP			NNP			EAS			EQI			SAS			Total	
	Pi	d18Oi	d18Oi*(Pi/P)	Pi	d18Oi	d18Oi*(Pi/P)	Pi	d18Oi	d18Oi*(Pi/P)	Pi	d18Oi	d18Oi*(Pi/P)	Pi	d18Oi	d18Oi*(Pi/P)	P	d18O
Pmax	0.99	-11.26	-3.43	0.44	-4.49	-0.62	1.31	-5.32	-2.16	0.2773	-16.81	-1.44	0.215	-16.67	-1.11	3.24	-8.76
Pmin	1.01	-12.31	-4.34	0.34	-4.07	-0.48	1.16	-4.13	-1.68	0.1955	-19.36	-1.32	0.159	-19.09	-1.06	2.86	-8.88
Pmin - Pmax	0.023		-0.91			0.14			0.48			0.12		0.05		-0.37	-0.12
Pmax	0.99	-11.26	-4.05	0.44	-4.49	-0.73	1.31	-5.32	-2.55							2.74	-7.32
Pmin	1.01	-12.31	-4.96	0.34	-4.07	-0.55	1.16	-4.13	-1.91							2.51	-7.42
Pmin - Pmax	0.023		-0.91			0.18			0.63							-0.23	-0.09
Summer	Pi	d18Oi	d18Oi*(Pi/P)	Pi	d18Oi	d18Oi*(Pi/P)	Pi	d18Oi	d18Oi*(Pi/P)	Pi	d18Oi	d18Oi*(Pi/P)	Pi	d18Oi	d18Oi*(Pi/P)	P	d18O
Pmax	1.60	-7.48	-2.41	0.37	-4.18	-0.31	1.76	-4.67	-1.66	0.73	-10.26	-1.50	0.502	-9.54	-0.97	4.96	-6.85
Pmin	2.00	-5.76	-2.20	0.23	-5.53	-0.24	1.87	-3.78	-1.35	0.63	-13.35	-1.61	0.518	-12.56	-1.24	5.24	-6.63
Pmin - Pmax	0.400		0.22			0.07			0.31			-0.11		-0.28		0.28	0.22

(b) dD																	
Annual	SNP			NNP			EAS			EQI			SAS			Total	
	Pi	dDi	dDi*(Pi/P)	Pi	dDi	dDi*(Pi/P)	Pi	dDi	dDi*(Pi/P)	Pi	dDi	dDi*(Pi/P)	Pi	dDi	dDi*(Pi/P)	P	d18O
Pmax	0.99	-78.75	-28.33	0.44	-22.89	-3.71	1.31	-30.03	-14.36							2.74	-46.40
Pmin	1.01	-87.61	-35.27	0.34	-20.25	-2.72	1.16	-21.30	-9.86							2.51	-47.85
Pmin - Pmax	0.023		-6.94			0.99			4.49							-0.23	-1.45
Summer	Pi	dDi	dDi*(Pi/P)	Pi	dDi	dDi*(Pi/P)	Pi	dDi	dDi*(Pi/P)	Pi	dDi	dDi*(Pi/P)	Pi	dDi	dDi*(Pi/P)	P	Total
Pmax	1.60	-49.11	-15.85	0.37	-25.20	-1.88	1.76	-28.64	-10.17	0.73	-74.25	-10.86	0.502	-68.43	-6.93	4.96	-45.69
Pmin	2.00	-38.14	-14.56	0.23	-35.55	-1.53	1.87	-24.57	-8.74	0.63	-95.66	-11.54	0.518	-89.5	-8.85	5.24	-45.21
Pmin - Pmax	0.400		1.29			0.35			1.42			-0.67		-1.92		0.28	0.48

(c) d-excess																	
Annual	SNP			NNP			EAS			EQI			SAS			Total	
	Pi	dex_i	dex_i*(Pi/P)	Pi	dex_i	dex_i*(Pi/P)	Pi	dex_i	dex_i*(Pi/P)	Pi	dex_i	dex_i*(Pi/P)	Pi	dex_i	dex_i*(Pi/P)	P	dexc
Pmax	0.99	11.33	4.08	0.44	13.00	2.11	1.31	12.55	6.00							2.74	12.19
Pmin	1.01	10.87	4.38	0.34	12.29	1.65	1.16	11.76	5.45							2.51	11.47
Pmin - Pmax	0.023		0.30			-0.46			-0.55							-0.23	-0.71
Summer	Pi	dex_i	dex_i*(Pi/P)	Pi	dex_i	dex_i*(Pi/P)	Pi	dex_i	dex_i*(Pi/P)	Pi	dex_i	dex_i*(Pi/P)	Pi	dex_i	dex_i*(Pi/P)	P	Total
Pmax	1.60	10.73	3.46	0.37	8.20	0.61	1.76	8.70	3.09	0.73	7.83	1.15	0.502	7.89	0.80	4.96	9.11
Pmin	2.00	7.94	3.03	0.23	8.71	0.37	1.87	5.67	2.02	0.63	11.14	1.34	0.518	10.98	1.09	5.24	7.85
Pmin - Pmax	0.400		-0.43			-0.24			-1.07			0.20		0.29		0.28	-1.26

164

Table S3: Korean Speleothem- $\delta^{18}O$ records.

(a) Eden Cave		(b) Gwaneum Cave	
Age (ka BP)	$\delta^{18}O$ (‰, VPDB)	Age (ka BP)	$\delta^{18}O$ (‰, VPDB)
128.19	-7.14	89.00	-8.95
127.77	-7.04	88.83	-8.98
127.34	-7.21	88.66	-8.81
126.49	-7.18	88.49	-9.04
126.06	-7.09	88.32	-9.00
125.63	-7.37	88.15	-8.78
125.21	-7.22	87.98	-8.66
124.78	-7.58	87.81	-8.70
124.36	-7.54	87.64	-8.48
123.93	-7.65	87.47	-8.57
123.50	-7.39	87.30	-8.70
123.08	-7.45	87.13	-8.56
122.22	-7.13	86.96	-8.76
121.80	-6.91	86.79	-8.67
121.37	-7.13	86.62	-8.63
120.94	-6.93	86.45	-8.60
120.52	-7.15	86.28	-8.58
120.09	-6.93	86.11	-8.82
119.66	-7.13	85.94	-8.84
119.24	-7.12	85.77	-8.77
118.81	-7.47	85.60	-8.74
118.39	-7.48	85.43	-8.52
117.96	-7.65	85.26	-8.78
117.53	-7.80	85.09	-8.61
117.11	-8.11	84.92	-8.37
116.68	-7.20	84.75	-8.32
116.25	-8.13	84.58	-8.25
115.83	-8.12	84.41	-8.43
115.40	-8.10	84.24	-8.79
114.97	-7.94	84.07	-8.58
114.55	-8.08	83.90	-8.59
114.12	-7.84	83.73	-8.60
113.70	-8.12	83.56	-8.34
113.27	-8.07	83.39	-8.13
112.84	-8.08	83.22	-8.27
112.42	-8.04	83.05	-8.39
111.99	-8.32	82.88	-8.18
111.56	-8.16	82.71	-8.40
111.14	-8.02	82.54	-8.64

110.71	-8.04	82.37	-8.52
110.28	-8.04	82.20	-8.49
108.70	-7.78	82.03	-8.37
107.12	-8.07	81.86	-8.32
105.54	-7.59	81.69	-8.38
103.96	-8.10	81.52	-8.17
102.38	-7.66	81.35	-8.21
100.80	-8.31	81.18	-8.24
		81.01	-8.25
209.89	-7.90	80.84	-8.14
206.62	-7.85	80.67	-8.27
204.98	-7.83	80.50	-8.27
203.35	-7.89	80.33	-8.53
201.71	-7.60	80.16	-8.03
200.08	-7.82	79.99	-8.36
199.54	-8.38	79.82	-8.47
199.01	-8.08	79.65	-8.20
198.47	-7.94	79.48	-8.29
197.93	-7.95	79.31	-8.40
197.40	-7.04	79.14	-8.30
196.86	-8.26	78.97	-8.57
196.33	-8.13	78.80	-8.56
195.79	-7.87	78.63	-8.63
195.26	-7.94	78.46	-8.54
194.72	-8.17	78.29	-8.46
194.18	-7.97	78.12	-8.35
193.65	-7.58	77.95	-8.75
193.11	-8.06	77.78	-8.41
192.58	-8.42	77.61	-8.43
192.04	-7.80	77.44	-8.34
191.51	-8.23	77.27	-8.36
190.97	-8.32	77.10	-8.37
190.43	-8.37	76.93	-8.30
189.90	-8.23	76.76	-8.39
189.36	-8.33	76.59	-8.25
189.10	-8.09	76.42	-8.38
188.83	-8.05	76.25	-8.25
188.57	-7.66	76.08	-8.15
188.31	-7.75	75.91	-8.03
188.04	-7.55	75.74	-7.94
187.78	-7.47	75.57	-7.92
187.51	-7.42	75.40	-8.19
187.25	-7.26	75.23	-7.86

186.98	-6.90	75.06	-8.29
186.72	-7.09	74.89	-8.22
186.45	-6.98	74.72	-8.18
186.19	-6.98	74.55	-8.21
185.93	-6.92	74.38	-8.31
185.66	-7.11	74.21	-8.23
185.40	-7.72	74.04	-8.15
185.13	-7.97	73.87	-8.33
184.87	-8.03	73.70	-8.10
184.60	-7.81	73.53	-8.02
		73.36	-8.11
441.84	-7.77	73.19	-8.05
441.72	-7.90	73.02	-7.77
441.60	-7.63	72.85	-7.94
441.48	-7.64	72.68	-8.19
441.36	-7.62	72.51	-8.01
441.24	-7.61	72.34	-7.74
441.13	-7.66	72.17	-8.20
441.01	-7.79	72.00	-8.25
440.89	-7.35	71.83	-8.23
440.77	-7.44	71.66	-8.24
440.65	-6.92	71.49	-8.30
440.53	-6.97		
440.42	-6.67	1.18	-8.45
440.30	-6.70	1.12	-8.50
440.18	-6.63	1.06	-8.70
440.06	-6.37	1.00	-8.16
439.94	-6.04	0.94	-8.32
439.82	-6.32	0.88	-7.77
439.71	-6.21	0.82	-8.24
439.59	-6.44	0.76	-7.68
439.47	-6.03	0.70	-7.78
439.35	-7.01		
439.23	-7.61		
439.11	-8.63		
439.00	-8.60		
438.88	-8.15		
438.64	-8.30		
438.52	-8.83		
438.40	-8.78		
438.17	-8.99		
438.05	-8.50		
437.93	-8.94		

437.81	-8.56
437.69	-8.67
437.58	-7.73
437.46	-8.21
437.22	-8.03
436.99	-8.58
436.76	-8.51
436.52	-8.54
436.29	-8.22
436.06	-8.40
435.82	-8.69
435.59	-9.14
435.36	-9.08
435.12	-8.66
434.89	-8.20
434.66	-8.43
434.42	-8.30
434.19	-8.79
433.96	-8.72
433.72	-8.83
433.49	-8.52
433.26	-8.96
433.02	-8.63
432.79	-8.85
432.56	-8.69
432.32	-9.01
432.09	-8.68
431.86	-8.95
431.62	-8.51
431.39	-8.62
431.16	-8.55
430.92	-8.61
430.69	-8.69
430.46	-8.87
430.22	-8.65
429.99	-8.81
429.76	-8.89
429.52	-8.55
429.29	-8.26
429.06	-8.67
428.82	-8.50
428.59	-8.92
428.36	-8.74

428.12	-8.84
427.89	-8.60
427.66	-8.47
427.42	-8.42
427.19	-8.63
426.96	-8.71
426.72	-8.77
426.49	-8.68
426.26	-8.49
425.35	-8.61
424.44	-8.67
423.53	-8.28
422.63	-8.34
421.72	-8.29
420.81	-8.34
419.90	-8.31
418.99	-8.69
418.09	-8.36
417.18	-8.27
416.27	-7.95
415.36	-8.12
414.45	-8.28
413.55	-8.96
412.64	-8.70
411.73	-8.27
410.82	-8.31
409.91	-8.29
409.00	-7.36
408.10	-8.13
407.19	-8.01
406.28	-7.94
405.37	-7.95
404.46	-8.28
403.56	-7.96
402.65	-7.96
401.74	-7.82
400.83	-8.26
399.92	-7.99
399.02	-8.11
398.11	-7.82
397.20	-7.71
529.99	-7.78

528.78	-7.73
527.57	-7.85
526.36	-7.58
525.15	-7.83
523.94	-7.25
522.73	-7.74
521.52	-8.09
520.31	-8.37
519.10	-8.24
517.89	-8.51
516.68	-8.31
515.47	-8.03
514.26	-7.87
513.04	-7.93
511.83	-7.77
510.62	-7.90
509.41	-7.63
508.20	-7.64
506.99	-7.62
505.78	-7.61
504.57	-7.66
503.36	-7.79
502.15	-7.35
500.94	-7.44
499.73	-6.92
498.52	-6.97

167
168
169

170 **SI References**

171

172 Beck, J. W., Zhou, W., Li, C., Wu, Z., White, L., Xian, F., Kong, X., and An,
173 Z.: A 550,000-year record of East Asian monsoon rainfall from ¹⁰Be in loess,
174 Science, 360, 877–881, <https://doi.org/10.1126/science.aam5825>, 2018.

175 Cheng, H., Edwards, R. L., Sinha, A., Spötl, C., Yi, L., Chen, S., Kelly, M.,
176 Kathayat, G., Wang, X., Li, X., Kong, X., Wang, Y., Ning, Y., and Zhang, H.:
177 The Asian monsoon over the past 640,000 years and ice age terminations,
178 Nature, 534, 640–646, <https://doi.org/10.1038/nature18591>, 2016.

179 Hayashi, R., Takahara, H., Inouchi, Y., Takemura, K., and Igarashi, Y.:
180 Vegetation and endemic tree response to orbital-scale climate changes in the
181 Japanese archipelago during the last glacial–interglacial cycle based on pollen
182 records from Lake Biwa, western Japan, Review of Palaeobotany and
183 Palynology, 241, 85–97, <https://doi.org/10.1016/j.revpalbo.2017.02.008>, 2017.

184 Hayashi, R., Sagawa, T., Irino, T., and Tada, R.: Orbital-scale vegetation-ocean-
185 atmosphere linkages in western Japan during the last 550 ka based on a pollen
186 record from the IODP site U1427 in the Japan Sea, Quaternary Science
187 Reviews, 267, 107103, <https://doi.org/10.1016/j.quascirev.2021.107103>, 2021.

188 Igarashi, Y. and Oba, T.: Fluctuations in the East Asian monsoon over the last
189 144ka in the northwest Pacific based on a high-resolution pollen analysis of
190 IMAGES core MD01-2421, Quaternary Science Reviews, 25, 1447–1459,
191 <https://doi.org/10.1016/j.quascirev.2005.11.011>, 2006.

192 Jo, K., Woo, K. S., Lim, H. S., Cheng, H., Edwards, R. L., Wang, Y., Jiang, X.,
193 Kim, R., Lee, J. I., Yoon, H. I., and Yoo, K.-C.: Holocene and Eemian climatic
194 optima in the Korean Peninsula based on textural and carbon isotopic records
195 from the stalagmite of the Daeya Cave, South Korea, Quaternary Science
196 Reviews, 30, 1218–1231, <https://doi.org/10.1016/j.quascirev.2011.02.012>,
197 2011.

198 Jo, K., Woo, K. S., Yi, S., Yang, D. Y., Lim, H. S., Wang, Y., Cheng, H., and
199 Edwards, R. L.: Mid-latitude interhemispheric hydrologic seesaw over the past
200 550,000 years, Nature, 508, 378–382, <https://doi.org/10.1038/nature13076>,
201 2014.

202 Lüthi, D., Le Floch, M., Bereiter, B., Blunier, T., Barnola, J. M., Siegenthaler,
203 U., Raynaud, D., Jouzel, J., Fischer, H., Kawamura, K., and Stocker, T. F.:
204 NOAA/WDS Paleoclimatology - EPICA Dome C - 800KYr CO2 Data,
205 <https://doi.org/10.25921/XGZS-GD10>, n.d.

206 Tarasov, P. E., Nakagawa, T., Demske, D., Österle, H., Igarashi, Y., Kitagawa,
207 J., Mokhova, L., Bazarova, V., Okuda, M., Gotanda, K., Miyoshi, N., Fujiki, T.,
208 Takemura, K., Yonenobu, H., and Fleck, A.: Progress in the reconstruction of
209 Quaternary climate dynamics in the Northwest Pacific: A new modern analogue
210 reference dataset and its application to the 430-kyr pollen record from Lake
211 Biwa, *Earth-Science Reviews*, 108, 64–79,
212 <https://doi.org/10.1016/j.earscirev.2011.06.002>, 2011.

213 Wen, Q., Liu, Z., Jing, Z., Clemens, S. C., Wang, Y., Yan, M., Ning, L., and
214 Liu, J.: Grand dipole response of Asian summer monsoon to orbital forcing, *npj*
215 *Clim Atmos Sci*, 7, 202, <https://doi.org/10.1038/s41612-024-00749-4>, 2024.

216

217